Journal of Statistical Physics, Vol. 121, Nos. 1/2, October 2005 (© 2005)
DOI: 10.1007/s10955-005-8412-0

A Consistent Grid Coupling Method for Lattice-Boltzmann Schemes

Martin Rheinländer[1]

Received October 12, 2004; accepted July 19, 2005

A method of coupling grids of different mesh size is developed for classical Lattice-Boltzmann (LB) algorithms on uniform grids. The approach is based on an asymptotic analysis revealing suitable quantities equalized along the grid interfaces for exchanging information between the subgrids. In contrast to other couplings the method works without overlap zones. Moreover the grid velocity (Mach number) is not kept constant, as the time step depends not linearly but quadratically on the grid spacing. To illustrate the basic idea we use a simple LB algorithm solving the advection-diffusion equation. The proposed grid coupling is validated by numerical convergence studies indicating, that the coupling does not affect the second-order convergence behavior of the LB algorithm which is observed on uniform grids. In order to demonstrate its principal applicability to other LB models, the coupling is generalized to the standard D2P9 model for (Navier-)Stokes flow and tested numerically. As we use analytic tools different from the Chapman-Enskog expansion, the theoretical background material is given in two appendices. In particular, the results of numerical experiments are confirmed with a consistency analysis.

KEY WORDS: Lattice-Boltzmann; asymptotic analysis; grid coupling; local refinement.

1. INTRODUCTION

For more than one and a half decades Lattice-Boltzmann (LB) schemes have been developed mainly for fluid flow simulations (cf. refs. 1 and 2). Although they are not yet as much established as conventional solvers of finite-difference or finite-element type, they possess already a considerable popularity in numerical engineering. The origin of LB schemes goes back to a special class of cellular automata (lattice-gas); but they are also

[1]Universität Konstanz; e-mail: martin.rheinlaender@uni-konstanz.de

strongly inspired by statistical physics and can be interpreted as a procedure to mimic the motion of virtual fluid particles according to physically motivated rules. In fact, the parallel to the kinetics of gases constitutes a certain originality of LB methods.

Classical LB schemes rely on uniform grids that are cubic in the most popular cases. This excludes *a priori* the possibility of local grid refinement, which has been successfully applied since long in the context of many other schemes. Grid coupling offers a possibility to overcome this drawback. The principal idea consists in dividing the computational domain into uniformly discretized subregions, where each subdomain can have a different mesh size. In those subdomains where the numerical error is expected to be high, a fine grid is advantageous, whereas at other places a coarser grid is sufficient and makes the code faster. Along the interfaces the subgrids have to exchange information. This turns out to be a subtle task as the LB algorithm introduces artificial quantities as primary variables. These so-called populations vary in the first order with respect to the grid size h. If we do not want to spoil the second order accuracy of the LB algorithm on uniform grids, we can not simply exchange the populations at the grid interfaces, since this would generate an error of first order in h (confer last paragraph of Appendix B).

One possibility of grid coupling is suggested in three papers by Filippova and Hänel.[3–5] This approach is also taken up by other authors in more recent publications as refs. 6–8. The population function is split into a grid-independent equilibrium part and an grid-dependent non-equilibrium part given as the population minus the equilibrium. This yields approximately the first-order of the Chapman-Enskog expansion. Because of its grid-dependence, the non-equilibrium part has to be transformed from one grid to another by multiplication with a suitable factor (see ref. 4). In ref. 5 this condition is also related to the continuity of macroscopic (physical) quantities across the interface. As the computation of the equilibrium requires the knowledge of all populations, this approach works only with overlapping subgrids, such that any interface node can be associated with a (virtual) partner node of the other grid, where all populations are known.

In contrast, our approach is directly motivated by the continuity of macroscopic quantities at the interface, as they should not "feel" the artificial transition from one subgrid to the other. As the macroscopic quantities depend always linearly on the populations (moment functionals), this leads immediately to equations, that can be considered as a linear system for the unknown populations on adjacent subgrids. Therefore the coupling works with a sharp interface, i.e. no overlapping is required.

Unlike the cited papers we respect strictly the diffusive scaling. Besides the structural parameter θ of the equilibrium distribution, the only independent parameter being introduced by the LB discretization is the grid spacing h. The BGK relaxation parameter ω (collision frequency) depends exclusively on the physical parameter ν (diffusivity/viscosity) and not on h (θ is regarded as fixed). Hence ω does not vary from subgrid to subgrid. Another consequence, that distinguishes our coupling from existing ones, consists in the quadratical growth of time steps on refined subgrids: if the grid spacing is diminished by a factor of r, then r^2 iterations on the refined grid correspond to one iteration on the original grid. This means, that the grid velocity (grid spacing/time step) is not constant throughout the whole mesh but is increased on the refined subgrids by the factor r.

2. BRIEF DESCRIPTION OF LB SCHEMES AND THEIR ASYMPTOTIC ANALYSIS

The LB methods provide a class of explicit numerical schemes for solving certain initial boundary value problems in the field of partial differential equations. The specific PDE problem to be solved by the LB algorithm is referred to as the *target problem*. Typical examples are the Stokes and Navier-Stokes equation or the diffusion-advection equation. Quantities that are directly related to the solution of the target problem are called *macroscopic* quantities. Unlike most finite-difference or finite-elements methods, LB schemes do not use macroscopic quantities like the solution of the target problem as their primary variables.

Based on a strongly simplified particle dynamics, a LB method is essentially characterized by its *finite, normalized (w.r.t. the $\|\cdot\|_\infty$-norm) velocity space* $\mathcal{S}$. In the case of a cubic grid in the d-dimensional space $\mathbb{R}^d$ it is a subset of $\{-1, 0, 1\}^d$, satisfying certain symmetries (e.g. invariance under reflection at the origin). As $\mathcal{S}$ models the continuous velocity space of the Boltzmann equation, it is often apostrophized as the *model*. In order to distinguish them we use the shortcut DdP($\#\mathcal{S}$), where D stands for the *number of spatial dimensions d* and P for the *number of populations*, i.e. the number of discrete velocities $\#\mathcal{S}$.

The set of real-valued functions over $\mathcal{S}$ is a vector space $\mathcal{F}$, which can be identified with $\mathbb{R}^{\#\mathcal{S}}$ and whose elements are denoted by sans-serif characters. The most prominent example is the *population function* F_h, appearing in the LB equation as its unknown and primary variable. Note that the index h indicates its grid dependence concerning its domain of definition as well as its numerical value. F_h is considered as an $\mathcal{F}$-valued function over the h-dependent space and time grid. So we write it with

either two or three arguments depending on whether we have the whole $\#\mathcal{S}$-tuple in mind or just the component (*population*) for some $\mathbf{s} \in \mathcal{S}$. In allusion to the phase-space density occurring in the Boltzmann equation, the populations might be interpreted as pseudo-densities of $\#\mathcal{S}$ different types of particles. The velocities of these particles are given as h-dependent multiples of the elements in $\mathcal{S}$.

The scalar product of $\mathsf{m}, \mathsf{w} \in \mathcal{F}$ is defined by $\langle \mathsf{m}, \mathsf{w} \rangle := \sum_{\mathbf{s} \in \mathcal{S}} \mathsf{m}_{\mathbf{s}} \mathsf{w}_{\mathbf{s}}$. If m is a polynomial in $\mathbf{s}$, then $M_h := \langle \mathsf{F}_h, \mathsf{m} \rangle$ is called the associated *moment*. These quantities are of particular interest, since they approximate the macroscopic quantities (solution, derivatives, fluxes etc.) for suitably chosen m.

Adopting the *diffusive scaling*, the time increment per iteration is defined as the squared grid size. So, the temporal index n is associated with the time nh^2, while the spatial multiindex $\mathbf{i} \in \mathbb{Z}^d$ corresponds to the node at the position $h\mathbf{i}$. The evolution of the population function F_h is determined by the *(discrete) LB equation* with a BGK collision operator.

$$\mathsf{F}_h(n+1, \mathbf{i}+\mathbf{s}, \mathbf{s}) = \mathsf{F}_h(n, \mathbf{i}, \mathbf{s}) + \omega\big[E_h\big(\mathsf{F}_h(n, \mathbf{i})\big) - \mathsf{F}_h(n, \mathbf{i})\big]_{\mathbf{s}} + h^2 \mathsf{Q}(n, \mathbf{i}, \mathbf{s}) \tag{1}$$

The relaxation parameter ω is related to a parameter of the target equation. Q is a known source term, that does not depend numerically on h. An important role comes up to the equilibrium operator $E_h \colon \mathcal{F} \to \mathcal{F}$. Usually it is given in terms of a linear or non-linear function of one or several moments, and therefore it depends only indirectly on the population function. Note that the evaluation of the equilibrium requires the knowledge of all $\#\mathcal{S}$ populations; that is why the equations for different populations are coupled with one another.

In order to start the algorithm described by (1), F_h is initialized in a special way by means of the initial data of the target problem (see for instance Eq. (8)). Furthermore the LB equation must be supplemented by boundary conditions; for our purpose, however, periodic boundary conditions are sufficient.

Since we are interested in the behavior of a numerical scheme for the discretization parameter h tending to zero, it is reasonable to analyze it with asymptotic techniques. For this, the Chapman-Enskog expansion is still a widely acknowledged tool in the LB context. However, we use here a simpler *regular expansion* with respect to the grid size h. This idea has been presented recently in refs. 9 and 10. Let us roughly sketch the procedure here. Detailed computations for several LB models will be found in ref. 12. Assume that there are smooth, $\mathcal{F}$-valued functions $\mathsf{f}^{(k)}$, $k \in \mathbb{N}_0$, of the non-discretized time space domain such that:

$$\mathsf{F}_h(n,\mathbf{i}) = \mathsf{f}^{(0)}(nh^2,\mathbf{i}h) + h\mathsf{f}^{(1)}(nh^2,\mathbf{i}h) + h^2\mathsf{f}^{(2)}(nh^2,\mathbf{i}h) + \cdots \tag{2}$$

We insert this ansatz into the LB equation and expand all terms completely with respect to h. In particular we have to replace the left hand side of (1) by a formal Taylor expansion. This enables us to compare coefficients leading thus to equations, that give the asymptotic orders $\mathsf{f}^{(k)}$ in terms of their locally conserved moments appearing in the equilibrium. In this way, we see how the LB method is related to the target problem and also what macroscopic quantities are hidden behind the numerical population function F_h and how they can be extracted. Thus we obtain also crucial hints for the design of coupling conditions.

The reader might be referred to the Appendix A, where we show exemplarily for the D1P3 model, that a truncated expansion in the form of (2) exists.

3. THE GRID COUPLING ALGORITHM FOR THE D1P3 MODEL

Due to its simplicity the D1P3 model is particularly useful for the development of new (coupling) algorithms as well as for demonstrational purposes. The advective term in the equilibrium permits us to test the robustness of the coupling by letting a disturbance cross the refined zone (see benchmark II, Fig. 2). This might be interesting, since a simple standard benchmark like the Poiseuille flow is only driven by diffusive, respectively, viscous effects. Moreover the Poiseuille flow is as well one-dimensional in its character.

Our target problem will be the following initial value problem for the diffusion-advection equation on an interval $[0, L]$ with periodic boundary conditions:

$$\begin{aligned} u(0,\cdot) &= u_0, \\ \partial_t u + a\partial_x u - \nu\partial_x^2 u &= q. \end{aligned} \tag{3}$$

The *advection velocity* a, and the *diffusivity* $\nu > 0$ are supposed to be constants. q represents a source while the initial value is given by u_0.

The finite velocity space of the D1P3 model is given by $\mathcal{S} := \{-1, 0, 1\} \equiv \{\ominus, 0, \oplus\}$. With $\mathsf{1}, \mathsf{s} \in \mathcal{F}$ we denote the constant one-function and the identity on $\mathcal{S}$. The equilibrium operator E_h, being linear like the target equation, is composed of a mandatory diffusive part and an advective part scaled by the grid size h; E_h acts on the nodal population vector F_h as a kind of projector in the following way:

$$E_h\mathsf{F}_h := \langle \mathsf{F}_h, \mathsf{1}\rangle \mathsf{w} + ha\langle \mathsf{F}_h, \mathsf{1}\rangle \theta \mathsf{s}\mathsf{w} \qquad \text{with } \mathsf{w} := (1-\mathsf{s}^2)\tfrac{\theta-1}{\theta} + \tfrac{1}{2\theta}\mathsf{s}^2. \tag{4}$$

Thus the equilibrium depends only on the *zeroth moment* also denoted as the *mass moment*, which corresponds to the sum of the three populations. The algorithmic parameter $\theta \geqslant 1$ is arbitrary but supposed to be fixed. Note that for $\theta = 1$ the rest population (velocity 0) is decoupled and we obtain actually a two population model. Let us introduce two macroscopic quantities

$$f := au - (\nu + \tfrac{1}{2\theta})\partial_x u, \tag{5}$$

$$g := \partial_x \big(au - \nu\, \partial_x u\big). \tag{6}$$

The quantity $f = f(t,x)$ is closely related to the physical *flux*, which is obtained by omitting $1/2\theta$ in its definition. $g = g(t,x)$ is the derivative of the physical flux. Observe that f and g correspond, apart from constant factors, to the first, respectively, second derivative of u, if the advection velocity a vanishes.

Assume the LB source term to be given by $\mathsf{Q}(n,i) = q(nh^2, ih)\mathsf{w}$. The diffusivity ν and the two LB parameters ω, θ shall be associated to each other by the formula

$$\nu = \tfrac{1}{\theta}\big(\tfrac{1}{\omega} - \tfrac{1}{2}\big). \tag{7}$$

Furthermore the population function F_h is supposed to be initialized according to the grid independent part of the equilibrium (zeroth order), which is the standard initialization, plus additional terms (first and second order) inhibiting strong initial layers and ensuring hence a smooth "start".

$$\mathsf{F}_h(0,i) = \underbrace{u(0,ih)\mathsf{w}}_{\text{0th order}} + h\underbrace{f(0,ih)\theta\mathsf{sw}}_{\text{1st order}} + h^2\underbrace{g(0,ih)\tfrac{1}{\omega}(1-\theta\mathsf{s}^2)\mathsf{w}}_{\text{2nd order}}. \tag{8}$$

Under appropriate smoothness conditions we can prove the following convergence results:

$$u(nh^2, ih) = \big\langle \mathsf{F}_h(nh^2, ih),\, \mathsf{1}\big\rangle + \mathrm{O}(h^2), \tag{9}$$

$$f(nh^2, ih) = \tfrac{1}{h}\big\langle \mathsf{F}_h(nh^2, ih), \mathsf{s}\big\rangle + \mathrm{O}(h^2), \tag{10}$$

$$\tfrac{\omega}{\theta - 1} g(nh^2, ih) = \tfrac{1}{h^2}\big\langle \mathsf{F}_h(nh^2, ih),\, \mathsf{s}^2 - \tfrac{1}{\theta}\big\rangle + \mathrm{O}(h^2). \tag{11}$$

This means that the mass moment converges quadratically to the solution u of the diffusion-advection equation. In contrast, the first and second moment converge to zero. However, if they are unscaled (i.e. in leading

order grid independent) by the division with a suitable power of h, they exhibit the very same convergence behavior to the flux-like quantity f, respectively, to the derivative of the flux g times the factor $\frac{\omega}{\theta-1}$. A full derivation of these results will be found in ref. 12 but the essential steps are sketched also in Appendix A.

Let us now consider a configuration as depicted in Fig. 1 with a refinement zone between $\zeta, \xi \in [0, L]$. It is assumed, that the coarse grid spacing $r\eta$ with $r \in \mathbb{N}$ and the fine grid spacing η match with the length of the subintervals. The population functions on the coarse and fine grid are denoted by G_η and K_η, respectively. In principle, the standard LB algorithm is performed independently on each of the subgrids. However, at the interface not all populations can be updated as prescribed by the LB equation (1), since an interfacial node has only one neighbor belonging to its own grid. The situation is shown in more detail for the left interface (cf. Fig. 1). Black arrows mark the populations $\mathsf{G}_\oplus, \mathsf{K}_\ominus$, that are *filled* by the standard update rule, whereas white arrows represent the populations $\mathsf{G}_\ominus, \mathsf{K}_\oplus$ remaining *empty*. The rest populations at the interface (not indicated in the figure) are updated in the usual way. Note, that, for convenience, we sometimes write the population specifiers $\{\ominus, 0, \oplus\}$ as indices, suppressing instead the dependence on the grid spacing. On both subgrids the zeroth moments should approximate the solution u of the target problem. For an ideal grid coupling we would expect the error on the coarse grid to be r^2 larger than on the fine grid due to the quadratic convergence. So Eq. (9) should become

$$\begin{aligned} u &= \langle \mathsf{G}_\eta, \mathsf{1} \rangle + \mathrm{O}(r^2\eta^2) \qquad \text{on the coarse subgrid,} \\ u &= \langle \mathsf{K}_\eta, \mathsf{1} \rangle + \mathrm{O}(\eta^2) \qquad \text{on the fine subgrid.} \end{aligned}$$

By subtracting these equations at the interface, where u is assumed to be continuous, we obtain

$$0 = \langle \mathsf{G}_\eta, \mathsf{1} \rangle - \langle \mathsf{K}_\eta, \mathsf{1} \rangle + \overbrace{\mathrm{O}(r^2\eta^2) - \mathrm{O}(\eta^2)}^{=\mathrm{O}(\eta^2)},$$

keeping in mind that r is a constant and thus independent of η. So the mass moments at the two coupling nodes are equal up to a term of the order $\mathrm{O}(\eta^2)$. As a first coupling condition for determining the empty populations we could therefore impose the equality of the mass moments. Since the committed error is then of the same order as the general discretization error of the LB algorithm itself, the coupling condition should be at least second-order consistent and not modify the quadratic convergence rate.

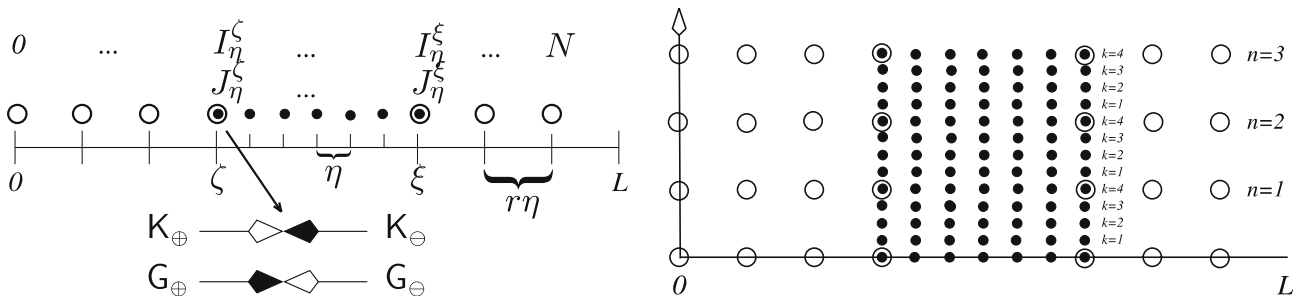

Fig. 1. The left sketch illustrates the grid geometry with a refinement factor $r = 2$. Due to the periodic boundary conditions, the right neighbor of the rightmost coarse grid node (index N) is given by the leftmost one and vice versa. On the right, the associated time space grid for three iterations on the coarse grid corresponding to $2^2 \times 3 = 12$ iterations on the fine grid is schematically displayed.

For a well behaved solution, we expect also the spatial derivative(s) to be continuous at the artificial grid interfaces ζ, ξ. In particular, this entails the continuity of the flux related quantity f. Arguing as above with

$$\begin{aligned} f &= \tfrac{1}{r\eta}\,\langle \mathsf{G}_\eta, \mathsf{s}\rangle + \mathrm{O}(r^2\eta^2) \quad \text{on the coarse subgrid,} \\ f &= \tfrac{1}{\eta}\,\langle \mathsf{K}_\eta, \mathsf{s}\rangle + \mathrm{O}(\eta^2) \quad \text{on the fine subgrid} \end{aligned}$$

yields a (multiplicative) jump in the first moments $\langle \mathsf{G}_\eta, \mathsf{s}\rangle, \langle \mathsf{G}_\eta, \mathsf{s}\rangle$ by the factor $1/r$:

$$\tfrac{1}{\eta}\langle \mathsf{K}_\eta, \mathsf{s}\rangle = \tfrac{1}{r\eta}\langle \mathsf{G}_\eta, \mathsf{s}\rangle + \mathrm{O}(\eta^2).$$

The reasoning might be summarized as follows:

$$\begin{array}{c}\text{continuity of } u \\ \&\ \partial_x u \text{ resp. } f \text{ at interface}\end{array} \quad \Rightarrow \quad \begin{array}{c}\text{equality of Zeroth moment} \\ \&\ \text{jump of First moment at interface.}\end{array}$$

Due to the diffusive scaling one time step on the coarse grid must correspond to r^2 time steps on the fine grid numbered by $1 \leqslant k \leqslant r^2$ (confer Fig. 1, right sketch). Thus, there are $r^2 - 1$ intermediate time steps on the fine grid, where necessary values for the coarse grid populations are missing. To overcome this lack, we apply linear interpolation in time. For $j \in \{I_\eta^\zeta, I_\eta^\xi\}$ (indices of the coarse grid interface nodes) we abbreviate:

$$\tilde{\mathsf{G}}_\eta\big(r^2(n-1)+k, j, s\big) := \tfrac{r^2-k}{r^2}\mathsf{G}_\eta(n-1, j, s) + \tfrac{k}{r^2}\mathsf{G}_\eta(n, j, s). \tag{12}$$

Ignoring for brevity the cumbersome index-arguments, we are led by our heuristic reasoning to the following implicit coupling conditions:

$$\text{(i)} \quad \langle \tilde{\mathsf{G}}_\eta, \mathsf{1}\rangle = \langle \mathsf{K}_\eta, \mathsf{1}\rangle \qquad \text{(ii)} \quad \tfrac{1}{r\eta}\langle \tilde{\mathsf{G}}_\eta, \mathsf{s}\rangle = \tfrac{1}{\eta}\langle \mathsf{K}_\eta, \mathsf{s}\rangle. \tag{13}$$

In order to obtain explicit coupling conditions, these equations are solved for the empty populations $\tilde{\mathsf{G}}_\ominus, \mathsf{K}_\oplus$ at the left interface and $\tilde{\mathsf{G}}_\oplus, \mathsf{K}_\ominus$ at the right interface. For the interface at ζ we get:

$$\begin{aligned} \tilde{\mathsf{G}}_\ominus - \mathsf{K}_\oplus &= \mathsf{K}_0 + \mathsf{K}_\ominus - \tilde{\mathsf{G}}_0 - \tilde{\mathsf{G}}_\oplus \\ \underbrace{\tilde{\mathsf{G}}_\ominus + r\mathsf{K}_\oplus}_{\text{empty}} &= \underbrace{r\mathsf{K}_\ominus + \tilde{\mathsf{G}}_\oplus}_{\text{known}} \end{aligned} \quad \Rightarrow \quad \text{system-matrix: } \begin{pmatrix} 1 & -1 \\ 1 & r \end{pmatrix}. \tag{14}$$

The system is uniquely solvable, since its matrix is invertible for every $r \in \mathbb{N}$. Note, that we are interested in $\tilde{\mathsf{G}}_\ominus$ at the left respectively $\tilde{\mathsf{G}}_\oplus$ at the right interface only for $k = r^2$.

For the trivial case $r = 1$, where both subgrids have equal mesh size, we need no time interpolation; hence $\tilde{\mathsf{G}}_s = \mathsf{G}_s$ for $s \in \{\ominus, 0, \oplus\}$. If the corresponding populations at the interface are equally initialized, we can show by induction, that we have $\mathsf{G}_0 = \mathsf{K}_0$ for every time step. Exploiting this gives $\mathsf{G}_\ominus = \mathsf{K}_\ominus$ and $\mathsf{K}_\oplus = \mathsf{G}_\oplus$. Thus the populations of the coarse grid and fine grid coupling node can be identified and the coupling algorithm simplifies to the standard update rule. This circumstance might be quite helpful for debugging an implementation (set $r = 1$ and compare with the algorithm on uniform grid).

The time loop of the LB algorithm with grid coupling takes now the following form:

for $n = 1 : maximal\_Iteration$,
- memorize interface populations needed for time interpolation: $\mathsf{G}_0(n-1, I_\eta^\zeta), \mathsf{G}_\oplus(n-1, I_\eta^\zeta), \mathsf{G}_0(n-1, I_\eta^\xi), \mathsf{G}_\ominus(n-1, I_\eta^\xi)$;
- standard update on coarse grid;
- **for** $k = 1 : r^2$,
  - standard update on fine grid;
  - computation of the empty fine grid interface populations: $\mathsf{K}_\oplus(r^2(n-1)+k, J_\eta^\zeta), \mathsf{K}_\ominus(r^2(n-1)+k, J_\eta^\xi)$;
- **end**;
- computation of the empty coarse grid interface populations: $\mathsf{G}_\ominus(n, I_\eta^\zeta), \mathsf{G}_\oplus(n, I_\eta^\xi)$;

end;

In order to study the behavior of the grid coupling let us consider two test examples on the time-space domain $[0, T] \times [0, L] = [0, 2] \times [0, 1]$. The analytic solutions are specified in Fig. 2. Benchmark (I) represents a simple diffusive decay (damped sine), whereas benchmark (II) is rather advective in its nature (traveling cosine). Disturbing effects of initial layers are reduced by the initialization (8) up to first order for benchmark (I) and even up to second order for benchmark (II). We set $h = r\eta$ on the coarse grid and $h = \eta$ on the fine grid. Furthermore we have set $\theta = 3$ and $r = 2$.

In Fig. 3 we present a numeric convergence study for both benchmarks. The coupled grid with the lowest resolution is displayed in Fig. 2, at the bottom left. This grid has been globally refined by a factor of $2, 3, \ldots$ up to 8. The error was measured in the supremum norm over the whole time space domain. So, it represents the maximal deviation from the exact values in all nodes and over all time steps. In both cases the

(I) $$\begin{cases} u(t,x) = e^{-36\pi^2\nu t}\sin(6\pi x) \\ \nu = 0.005\,, \quad a = 0 \end{cases}$$

(II) $$\begin{cases} u(t,x) = \cos(2\pi(x-at)) \\ q(t,x) = 4\pi^2\nu\cos(2\pi(x-at)) \\ \nu = 0.001\,, \quad a = 1.333 \end{cases}$$

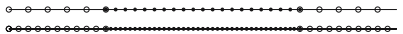

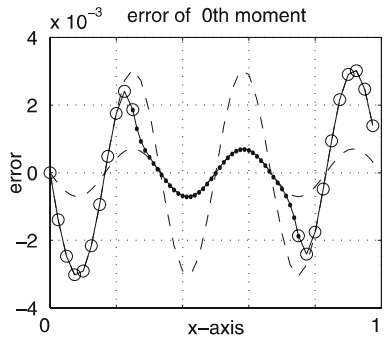

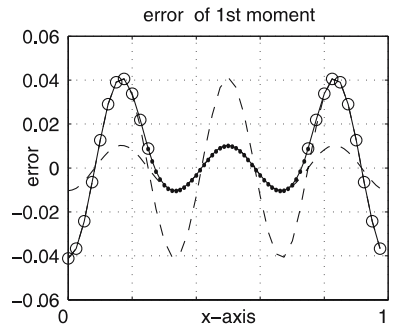

Fig. 2. Left above: Analytic solutions of the two benchmark problems. Left below: First and second grid of the grid sequence used for determining the convergence rates. The local refinement factor r is always 2. For the mth grid we have set $\eta = \frac{1}{40m}$ (mesh size of the fine grid). Center and Right: Snapshot of the error in the solution (zeroth moment) and the error in the flux (first moment) for the first benchmark problem after 160 iterations (t=0.1) on the second grid. The flat and steep dashed curves represent the error on an uniform coarse and fine grid, respectively, at the same time. The error curve on the coupled grid fits nicely between the two dashed curves.

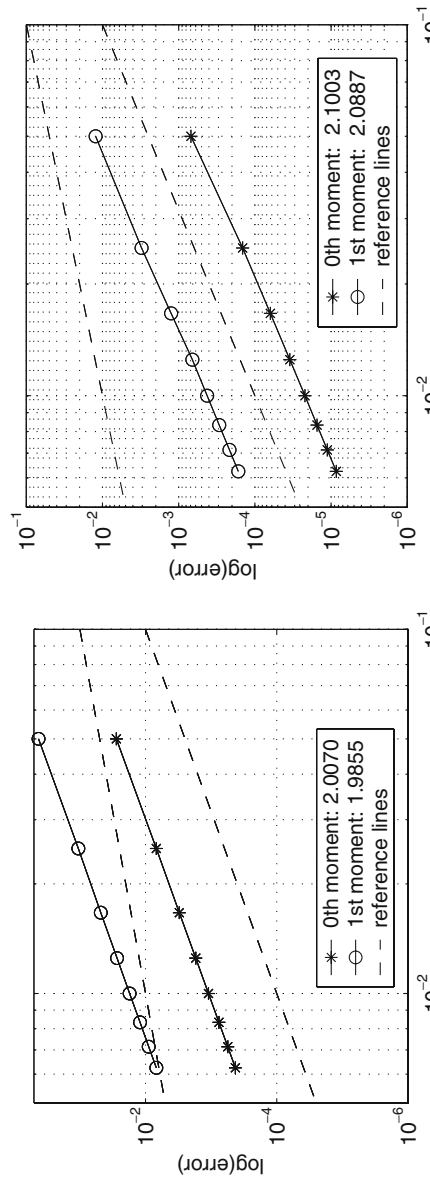

Fig. 3. Double logarithmic plot of the error versus the coarse grid size $r\eta$. Benchmark I (left), II (right). For comparison the reference lines indicate a slope of 1 and 2.

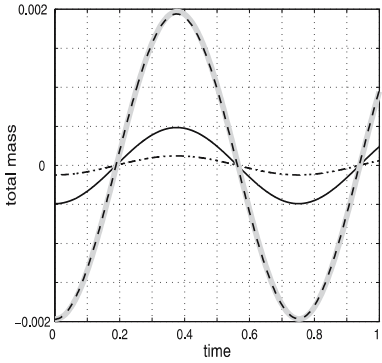

The total mass after the n'th time step (w.r.t. the coarse grid) is given by

$$r\eta \sum_{i,s} \mathsf{G}_\eta(n,i,s) + \eta \sum_{j,s} \mathsf{K}_\eta(r^2 n, j, s),$$

where the sums are to be taken over all nodes of the coarse resp. fine grid (indices i resp. j) and over all populations $s \in \mathcal{S}$. Note, that we multiply the sums by the corresponding grid spacing, as we deem the populations as densities.

Fig. 4. The change of total mass is displayed with respect to time for benchmark II. The curves refer to the first (dashed), second (solid) and fourth (dashed-dotted) mesh, where on each mesh as many iterations have been performed as are necessary to reach the time one. The amplitude reduces with the square of the grid spacing. The gray curve corresponds to the total mass of the exact solution u computed with the rectangle rule on the first mesh.

zeroth and first moment reveal a clear second-order convergence behavior. The mean convergence rates have been computed by a linear least square fit taking all eight grids into account. In Appendix B we will substantiate these observations theoretically by a consistency analysis of the coupling algorithm.

The *total mass* is defined as the integral of the solution of the target problem over the spatial domain, i.e. the interval $[0, L]$. Due to the periodic boundary conditions the total mass is a conserved quantity. In the two benchmark problems, it is equal to zero. Thanks to the symmetric position of the refined grid with respect to the sinusoidal initial value of u (benchmark I), the total mass is zero up to machine precision (less than 10^{-15}). Thus, the coupling algorithm does not noticeably affect the conservation of total mass in this example.

In contrast to simulations on uniform grids, the total mass is found slightly oscillating around the exact value in the advective case of the second benchmark. However this behavior is mainly related to the accuracy of the quadrature rule (rectangle rule, i.e. summing up the function values multiplied by the discretization spacing). In fact, if we integrate the exact solution also with the rectangle rule, we obtain almost the same curve (see Fig. 4).

4. AN OUTLOOK TOWARDS GRID COUPLING FOR THE D2P9 MODEL

Let us briefly demonstrate, that the grid coupling is extendible to other LB models too. For this we consider the D2P9 model, which has

evolved to the prevailing LB model for simulations of plane flows. What regards the finite velocity set $\mathcal{S}$, the weight function w, etc., we refer to ref. 2, p. 165 and also to ref. 9 for a more profound background concerning the equilibrium and the moment generating polynomials. It is sufficient for our purpose to take the linearized equilibrium

$$\begin{aligned} \mathcal{E}(P, V_x, V_y) &:= 3\mathsf{w}\left(V_x \mathsf{s}_x + V_y \mathsf{s}_y + h\, P\right), \\ P := \tfrac{1}{3h}\langle \mathsf{F}_h, \mathsf{1}\rangle, \quad V_x &:= \langle \mathsf{F}_h, \mathsf{s}_x\rangle, \quad V_y := \langle \mathsf{F}_h, \mathsf{s}_y\rangle \end{aligned} \tag{15}$$

that is a function of the unscaled mass moment P and the two first moments V_x, V_y. Note that $\mathsf{s}_x, \mathsf{s}_y \in \mathcal{F}$ assign to each $\mathbf{s} \in \mathcal{S}$ its x-, respectively, y-component. The target equation associated to this equilibrium is given by the incompressible Stokes equation:

$$\partial_t \mathbf{v} - \nu \Delta \mathbf{v} = -\nabla p, \quad \nabla \cdot \mathbf{v} = 0.$$

The function p denotes the pressure and $\mathbf{v} = (v_x, v_y)^T$ the velocity. They are approximated by P and (V_x, V_y), respectively. The viscosity ν is related to the collision frequency ω by $\nu = \frac{1}{3}(\frac{1}{\omega} - \frac{1}{2})$.

We consider the initial value problem for the target equation in the unit square with periodic boundary conditions. For the refinement zone, a rectangular patch is selected with parallel sides, shifted towards the south-west corner (see Fig. 5). Basically, the coupling algorithm can be

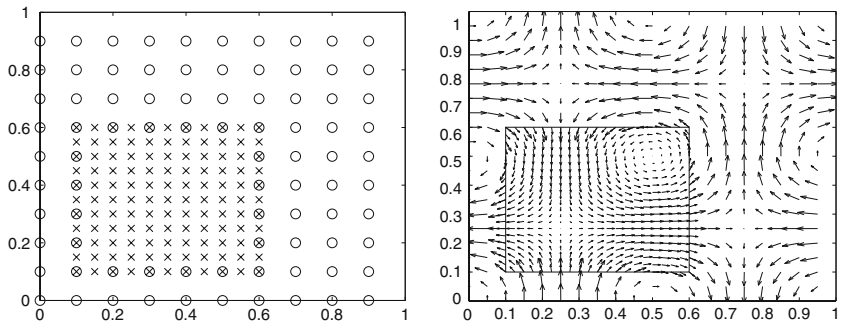

Fig. 5. Left: First grid of the grid sequence used for the convergence studies. Right: Velocity field on the second grid after 400 iterations ($t = 1$). For the decaying eigenmode of the Stokes operator (cf. Fig. 6), the velocity field basically does not change its appearance but only its strength. To be better recognizable the vectors are differently scaled in the fine and coarse grid domain.

Table I. Macroscopic quantities and their associated moment generating polynomials on $\mathcal{S}$. The scaling factors are used to rescale the moments, such that they become O(1) quantities, for example: $h^{-2}\langle \mathsf{F}_h, \mathsf{m}_{\phi_y}\rangle = h^{-2}(h^2\phi_y + \mathrm{O}(h^4)) = \phi_y + \mathrm{O}(h^2)$

Macroscopic quantity ($\tau := \omega^{-1}$)		Moment generating polynomial	Scaling
p	Pressure	$\mathsf{m}_p := \frac{1}{3}$	h^{-1}
v_x	x-component of velocity	$\mathsf{m}_{v_x} := \mathsf{s}_x$	1
v_y	y-component of velocity	$\mathsf{m}_{v_y} := \mathsf{s}_y$	1
σ_x	$:= p - \frac{2}{3}\tau\partial_x v_x$	$\mathsf{m}_{\sigma_x} := \mathsf{s}_x^2$	h^{-1}
σ_y	$:= p - \frac{2}{3}\tau\partial_y v_y$	$\mathsf{m}_{\sigma_y} := \mathsf{s}_y^2$	h^{-1}
σ_{xy}	$:= -\frac{1}{3}\tau(\partial_y v_x + \partial_x v_y)$	$\mathsf{m}_{\sigma_{xy}} := \mathsf{s}_x\mathsf{s}_y$	h^{-1}
ϕ_x	$:= \frac{2}{9}\tau(\tau - \frac{1}{2})(\partial_x^2 v_y + 2\partial_x\partial_y v_x)$	$\mathsf{m}_{\phi_x} := \mathsf{s}_x\mathsf{s}_y^2 - \frac{1}{3}\mathsf{s}_x$	h^{-2}
ϕ_y	$:= \frac{2}{9}\tau(\tau - \frac{1}{2})(\partial_y^2 v_x + 2\partial_x\partial_y v_y)$	$\mathsf{m}_{\phi_y} := \mathsf{s}_x^2\mathsf{s}_y - \frac{1}{3}\mathsf{s}_y$	h^{-2}
ψ	$:= -\frac{4}{9}\tau(\tau^2 - \tau + \frac{1}{6})\partial_x\partial_y(\partial_x v_y + \partial_y v_x)$	$\mathsf{m}_\psi := \mathsf{s}_x^2\mathsf{s}_y^2 - \frac{1}{3}(\mathsf{s}_x^2 + \mathsf{s}_y^2) + \frac{1}{9}$	h^{-3}

transferred straightforwardly. However, there are two new aspects: First, as the interface is a line instead of a single point, we encounter *hanging nodes*, i.e. interface nodes on the fine grid, that have no counterpart on the coarse grid. Therefore we introduce virtual partner nodes, whose populations are determined by spatial interpolation (with third-order polynomials) along the interface on the coarse grid. Second, *corner nodes* have to be treated in a special way.

The left column of Table I contains besides v_x, v_y, and p six further macroscopic quantities, that are accessible with second order accuracy by computing the moments associated to the indicated polynomials. Note that σ_x, σ_y and σ_{xy} would correspond to the stress tensor, if $\tau/3$ were replaced by ν in their definition. The last three quantities ϕ_x, ϕ_y and ψ have no direct physical interpretation.

Considering the grid configuration (cf. Fig. 5), we have to distinguish between *regular* interface nodes (including the hanging nodes) lying either on the interface parallel to the x- or y-axis and *corner* nodes. In the first case, fine grid and coarse grid interface nodes have three empty populations not updated by the standard propagation. In the latter case, the convex corner node (fine grid) has five empty populations, while the concave corner node (coarse grid) has only one. So the total number of unknowns is always six for any pair of coupling nodes. In order to determine them, we equate six out of the nine scaled moments listed in the table. However, the six moments can not be chosen arbitrarily, if the resulting linear system should be uniquely solvable. The subsequent choice satisfies this requirement.

Type of interface node	Equalized scaled moments
Horizontal ($\parallel x$-axis)	$V_x, V_y, \Sigma_y, \Sigma_{xy}, \Phi_y, \Psi$
Vertical ($\parallel y$-axis)	$V_x, V_y, \Sigma_x, \Sigma_{xy}, \Phi_x, \Psi$
Corner	$V_x, V_y, \Sigma_x, \Sigma_y, \Sigma_{xy}, \Psi$

N.B.: $\Sigma_x := h^{-1}\langle \mathsf{F}_h, \mathsf{m}_{\sigma_x}\rangle, \quad \Phi_x := h^{-2}\langle \mathsf{F}_h, \mathsf{m}_{\phi_x}\rangle$ etc.

To be more concrete we give here the coupling conditions on the boundaries parallel to the x-axis. The notation is chosen in direct analogy to the D1P3 coupling as in Eq. (13); remember that the swung dash over G indicates time interpolation.

$$\begin{aligned}
&\text{(i)} \quad \langle \tilde{\mathsf{G}}_\eta, \mathsf{m}_{v_x}\rangle = \langle \mathsf{K}_\eta, \mathsf{m}_{v_x}\rangle \qquad \text{(ii)} \quad \langle \tilde{\mathsf{G}}_\eta, \mathsf{m}_{v_y}\rangle = \langle \mathsf{K}_\eta, \mathsf{m}_{v_y}\rangle,\\
&\text{(iii)} \quad \tfrac{1}{r\eta}\langle \tilde{\mathsf{G}}_\eta, \mathsf{m}_{\sigma_y}\rangle = \tfrac{1}{\eta}\langle \mathsf{K}_\eta, \mathsf{m}_{\sigma_y}\rangle \qquad \text{(iv)} \quad \tfrac{1}{r\eta}\langle \tilde{\mathsf{G}}_\eta, \mathsf{m}_{\sigma_{xy}}\rangle = \tfrac{1}{\eta}\langle \mathsf{K}_\eta, \mathsf{m}_{\sigma_{xy}}\rangle,\\
&\text{(v)} \quad \tfrac{1}{(r\eta)^2}\langle \tilde{\mathsf{G}}_\eta, \mathsf{m}_{\phi_y}\rangle = \tfrac{1}{\eta^2}\langle \mathsf{K}_\eta, \mathsf{m}_{\phi_y}\rangle \qquad \text{(vi)} \quad \tfrac{1}{(r\eta)^3}\langle \tilde{\mathsf{G}}_\eta, \mathsf{m}_{\psi}\rangle = \tfrac{1}{\eta^3}\langle \mathsf{K}_\eta, \mathsf{m}_{\psi}\rangle.
\end{aligned}$$

Multiplying these scalar products out and sorting empty and known populations on the left and right-hand side, respectively, yields a 6×6 linear system being the counterpart of Eq. (14). Notice that the system matrix depends only on the type of the interface node (more exactly on which of the populations are empty) and is independent of the time iteration. Therefore its inverse can be computed once and for all before the LB algorithm starts.

The equating of the scaled moments is heuristically justified, if we assume the solution of the target equation sufficiently smooth, such that the given macroscopic quantities are continuous at the artificial interfaces.

It is remarkable, that the LB algorithm needs two more coupling conditions than we would obtain by a variational formulation of the target problem (6 versus 4, which are given by the continuity of both components of $\mathbf{v}$ and the normal stress, i.e. the stress tensor matrix times the normal vector of the interface). This is in opposition to the preceding D1P3 example, where both the target equation and the LB algorithm require two coupling conditions.

Finally, let us report a test problem provided by the decaying eigenmode of the Stokes operator (see Fig. 6, left). The convergence plot confirms numerically, that the LB scheme on the coupled grid is also of second order.

Because of grid-sampling effects similar to benchmark II in Section 3, we obtain also initial total velocities with respect to the x- and y-direction, that are slightly different from the analytic value 0 (e.g. around 1.66×10^{-3}

$$v_x(t,x,y) = -e^{-8\pi^2\nu t}\cos(2\pi x)\sin(2\pi y)$$
$$v_y(t,x,y) = \quad e^{-8\pi^2\nu t}\sin(2\pi x)\cos(2\pi y)$$
$$p(t,x,y) = 0\,, \qquad \nu = 0.01$$

Considered time space domain: $[0,2]\times[0,1]^2$.
Initialization:

$$\mathsf{F}_h(0,i,j,\mathbf{s}) = 3\mathsf{w}_\mathbf{s}\mathbf{s}\cdot\mathbf{v}_0(ih,jh) + 3h\mathsf{w}_\mathbf{s}\left[p_0(ih,jh) + \tfrac{1}{\omega}(\mathbf{s}\cdot\nabla)(\mathbf{s}\cdot\mathbf{v}_0(ih,jh))\right]$$

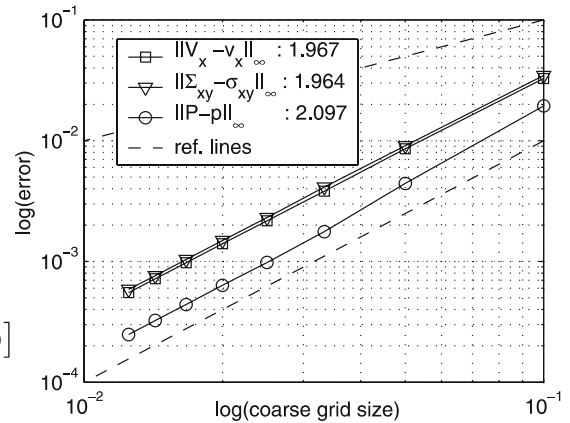

Fig. 6. Left: Analytic solution and initialization including first-order terms. Right: Convergence study by several global refinements of the original coupled grid. □: x-velocity component, nearly overlaid by ▽: off-diagonal stress tensor element, ◯: pressure. The average convergence rates w.r.t. to the supremum norm over the whole space time domain are in all three cases close to two.

for the first mesh). This effect reduces when the grid is refined. As long as the damping is perceptible, the total velocity components decrease with time. Notice, that the total x- resp. y-velocity is computed as the sum of V_x resp. V_y (cf. Eq. (15)) over all nodes of the coarse and fine subgrid multiplied by the squared grid spacing.

In this example, the total mass (total pressure which is the sum of P over all nodes) has initially a magnitude of 10^{-17}. However, a very slow increase is observed, that does not occur on a uniform grid.

5. APPENDIX A: CONSISTENCY OF THE LATTICE-BOLTZMANN ALGORITHM

Here we are going to justify the convergence results formulated in Eqs. (9)–(11) without entering into all details. The proof is based upon a *prediction function* $\hat{\mathsf{F}}_h$, that approximates or "predicts" the evolution of the population function F_h with a certain order of accuracy. A formal asymptotic expansion (cf. Eq. (2)) reveals, how the prediction function has to be chosen. However we prefer here a converse presentation, i.e. we indicate the construction without any further motivation and verify afterwards that it has the required properties. Afore, a preliminary consideration is necessary.

Let φ be a function depending on time and space. We want to approximate $\varphi(t+h^2, x+sh)$ by a truncated Taylor expansion. Therefore assume that φ is at least four times differentiable. If we rearrange the truncated Taylor series, such that terms of equal power in h are collected, and keep explicitly only those terms being of order three or less in h, we obtain

$$\varphi(t+h^2, x+sh) = \sum_{\alpha=0}^{3} h^\alpha\, T_\alpha(\partial_t, s\partial_x)\varphi(t,x) + \mathrm{O}(h^4).$$

This relation defines the bivariate polynomials T_α with $0 \leqslant \alpha \leqslant 3$. An easy computation yields

$$T_0(\vartheta, \varsigma) = 1, \qquad T_2(\vartheta, \varsigma) = \vartheta + \tfrac{1}{2}\varsigma^2,$$
$$T_1(\vartheta, \varsigma) = \varsigma, \qquad T_3(\vartheta, \varsigma) = \varsigma\vartheta + \tfrac{1}{6}\varsigma^3.$$

May now u be the solution of the initial value problem (3) for the advection-diffusion equation, where we set $q = 0$ to simplify the computations. We suppose u to be sufficiently smooth, such that the following functions are reasonably defined.

$$\left.\begin{aligned}
&\mathsf{f}^{(0)}(t,x,s) := u(t,x)\mathsf{w}_s,\\
&\mathsf{f}^{(1)}(t,x,s) := au(t,x)\theta s\mathsf{w}_s - \tfrac{1}{\omega}T_1(\partial_t, s\partial_x)\mathsf{f}^{(0)}(t,x,s),\\
&\mathsf{f}^{(2)}(t,x,s) := -\tfrac{1}{\omega}\big\{T_1(\partial_t, s\partial_x)\mathsf{f}^{(1)}(t,x,s) + T_2(\partial_t, s\partial_x)\mathsf{f}^{(0)}(t,x,s)\big\},\\
&\mathsf{f}^{(3)}(t,x,s) := -\tfrac{1}{\omega}\big\{T_1(\partial_t, s\partial_x)\mathsf{f}^{(2)} + T_2(\partial_t, s\partial_x)\mathsf{f}^{(1)} + T_3(\partial_t, s\partial_x)\mathsf{f}^{(0)}\big\}_{(t,x,s)}.
\end{aligned}\right\} \tag{16}$$

For later purposes let us already compute $\mathsf{f}^{(1)}, \mathsf{f}^{(2)}$ more explicitly. As abbreviation, it is convenient to use the macroscopic quantities f, g defined by Eqs. (5) and (6), respectively. Resolving the recursive definition of $\mathsf{f}^{(1)}$ leads to:

$$\begin{aligned}
\mathsf{f}^{(1)} &\overset{(16)}{=} au\theta\mathsf{sw} - \tfrac{1}{\omega}\mathsf{s}\partial_x u\mathsf{w} = \big(au - \tfrac{1}{\omega\theta}\partial_x u\big)\theta\mathsf{sw}\\
&\overset{(7)}{=} \big(au - (\nu + \tfrac{1}{2\theta})\partial_x u\big)\theta\mathsf{sw} \overset{(5)}{=} f\theta\mathsf{sw}.
\end{aligned}$$

Similarly we obtain:

$$\begin{aligned}
-\omega\mathsf{f}^{(2)} &\overset{(16)}{=} \mathsf{s}\partial_x f\theta\mathsf{sw} + \Big(\partial_t + \tfrac{1}{2}\mathsf{s}^2\partial_x^2\Big)u\mathsf{w}\\
&\overset{(5)}{=} \partial_x\big(au - (\nu + \tfrac{1}{2\theta})\partial_x^2 u\big)\theta\mathsf{s}^2\mathsf{w} + \partial_t u\mathsf{w} + \tfrac{1}{2\theta}\partial_x^2 u\theta\mathsf{s}^2\mathsf{w}\\
&\overset{(3)}{=} \partial_x\big(au - \nu\partial_x^2 u\big)\theta\mathsf{s}^2\mathsf{w} - \big(a\partial_x u - \nu\partial_x^2 u\big)\mathsf{w}\\
&= \partial_x\big(au - \nu\partial_x^2 u\big)\theta(\mathsf{s}^2 - \tfrac{1}{\theta})\mathsf{w} \overset{(6)}{=} g\theta(\mathsf{s}^2 - \tfrac{1}{\theta})\mathsf{w}.
\end{aligned}$$

The calculations are summarized by

$$\mathsf{f}^{(1)}(t,x) = f(t,x)\theta\mathsf{sw}, \qquad \mathsf{f}^{(2)}(t,x) = -\tfrac{1}{\omega}g(t,x)\theta(\mathsf{s}^2 - \tfrac{1}{\theta})\mathsf{w}. \tag{17}$$

We refer to $\mathsf{f}^{(\alpha)}$ $(0 \leqslant \alpha \leqslant 3)$ as the α'th *asymptotic order* of the *extended prediction function*

$$\hat{\mathsf{f}}_h := \mathsf{f}^{(0)} + h\mathsf{f}^{(1)} + h^2\mathsf{f}^{(2)} + h^3\mathsf{f}^{(3)}.$$

Now we are able to define the *(discrete) prediction function* by

$$\hat{\mathsf{F}}_h(m, j, s) := \hat{\mathsf{f}}_h(mh^2, jh, s)$$

for admissible time and space indices m, j. The assertion we want to prove in the sequel is, that $\hat{\mathsf{F}}_h$ satisfies the LB equation approximately, i.e. with a

residual vanishing quadratically with the discretization parameter h. More exactly:

$$\frac{1}{h^2}\left\{\hat{\mathsf{F}}_h(n,i,s)-\hat{\mathsf{F}}_h(n-1,i-s,s)-\omega\big[\big(E_h-I\big)\hat{\mathsf{F}}_h(n-1,i-s)\big]_s\right\}\stackrel{!}{=}\mathrm{O}(h^2). \tag{18}$$

Expressing this equation in terms of $\hat{\mathsf{f}}_h$, where we set for shortness

$$(n-1)h^2\leftrightarrow t,\qquad (i-s)h\leftrightarrow x,$$

we obtain equivalently:

$$\frac{1}{h^2}\left\{\hat{\mathsf{f}}_h(t+h^2,x+sh,s)-\hat{\mathsf{f}}_h(t,x,s)-\omega\big[(E_h-I)\hat{\mathsf{f}}_h(t,x)\big]_s\right\}\stackrel{!}{=}\mathrm{O}(h^2). \tag{19}$$

Notice, that the factor $1/h^2$ evokes the affinity to a differential equation. As h^2 corresponds to the time increment, the difference of the shifted and unshifted prediction function divided by h^2 approximates the convective derivative of $\hat{\mathsf{f}}_h$ in the direction of s, i.e. $\partial_t\hat{\mathsf{f}}_h+h^{-1}s\partial_x\hat{\mathsf{f}}_h$. Replacing formally the difference quotient by the convective derivative, yields a system of partial differential equations, that are *singularly* scaled because of the factors h^{-1} and h^{-2} appearing in front of the spatial derivative and the collision term, respectively. Of course, this PDE system has many things in common with the algorithm and is also of interest by its own (see ref. 11 in the context of the D2P9 model and ref. 12). This observation suggests, that it is advantageous for theoretical investigations *not* to write the LB equation in the form (1), as it is used for implementations. An important consequence of this is mentioned below.

In order to verify (19) let us first calculate the mass-moment and the equilibrium of $\hat{\mathsf{f}}_h$. Writing $\mathsf{f}^{(1)}$, $\mathsf{f}^{(3)}$ in terms of $\mathsf{f}^{(0)}$, respectively, u, we observe that all addends contain either s or $s^3=s$. As $\langle\mathsf{s},\mathsf{w}\rangle=\sum_{s\in\mathcal{S}}s\mathsf{w}_s=0$, the mass-moments of $\mathsf{f}^{(1)}$, $\mathsf{f}^{(3)}$ must vanish. Since $(\mathsf{s}^2-\frac{1}{\theta})\mathsf{w}$ is orthogonal to $\mathsf{1}$, the mass-moment of the second asymptotic order $\mathsf{f}^{(2)}$ vanishes too. This result is not at all obvious, if we take for $\mathsf{f}^{(2)}$ its definition in (16) instead of its representation in (17). We have made essential use of u being a solution of the diffusion-advection equation and of the ν-ω relation (7) in order to derive (17). Thus we get

$$\langle\hat{\mathsf{f}}_h,\mathsf{1}\rangle=\sum_{\alpha=0}^{3}h^\alpha\langle\mathsf{f}^{(\alpha)},\mathsf{1}\rangle=\langle\mathsf{f}^{(0)},\mathsf{1}\rangle=u, \tag{20}$$

which implies

$$\begin{aligned}\big[E_h\hat{\mathsf{f}}_h(t,x)\big]_s &:= \langle\hat{\mathsf{f}}_h(t,x),\mathsf{1}\rangle\mathsf{w}_s + ha\langle\hat{\mathsf{f}}_h(t,x),\mathsf{1}\rangle\theta s\mathsf{w}_s\\ &= u(t,x)\mathsf{w}_s + hau(t,x)\theta s\mathsf{w}_s.\end{aligned}$$

Comparing this with the definition of the asymptotic orders in (16), we are led to the subsequent representation of the extended prediction function

$$\hat{\mathsf{f}}_h(t,x,s) = \big[E_h\hat{\mathsf{f}}_h(t,x)\big]_s - \tfrac{1}{\omega}\sum_{\alpha=1}^{3} h^\alpha \sum_{\beta=1}^{\alpha} T_\beta(\partial_t, s\partial_x)\mathsf{f}^{(\alpha-\beta)}(t,x,s),$$

which immediately yields

$$\omega\big[(E_h - I)\hat{\mathsf{f}}_h(t,x)\big]_s = \sum_{\alpha=1}^{3} h^\alpha \sum_{\beta=1}^{\alpha} T_\beta(\partial_t, s\partial_x)\mathsf{f}^{(\alpha-\beta)}(t,x,s)\,. \tag{21}$$

Let us resort to our preliminary consideration to transform the temporarily and spatially shifted $\hat{\mathsf{f}}_h$ in (19). By the definition of the T_α's and of $\hat{\mathsf{f}}_h$ we find

$$\begin{aligned}\hat{\mathsf{f}}_h(t+h^2, x+sh, s) &= \sum_{\alpha=0}^{3} h^\alpha\, T_\alpha(\partial_t, s\partial_x)\hat{\mathsf{f}}_h(t,x,s) + \mathrm{O}(h^4)\\ &= \sum_{\alpha=0}^{3} h^\alpha \sum_{\beta=0}^{\alpha} T_\beta(\partial_t, s\partial_x)\mathsf{f}^{(\alpha-\beta)}(t,x,s) + \mathrm{O}(h^4).\end{aligned}$$

Combining this with (21) gives

$$\begin{aligned}&\hat{\mathsf{f}}_h(t+h^2, x+sh, s) - \omega\big[(E_h - I)\hat{\mathsf{f}}_h(t,x)\big]\\ &\quad= \sum_{\alpha=0}^{3} h^\alpha \sum_{\beta=0}^{0} T_\beta(\partial_t, s\partial_x)\mathsf{f}^{(\alpha-\beta)}(t,x,s) + \mathrm{O}(h^4)\\ &\quad= \sum_{\alpha=0}^{3} h^\alpha \mathsf{f}^{(\alpha)}(t,x,s) + \mathrm{O}(h^4) = \hat{\mathsf{f}}_h(t,x,s) + \mathrm{O}(h^4)\,.\end{aligned}$$

Since the obtained $\hat{\mathsf{f}}_h(t,x,s)$ is canceled by the remaining $-\hat{\mathsf{f}}_h(t,x,s)$ of Eq. (19), we see, that its left-hand side simplifies to $\mathrm{O}(h^4)$, which gives an $\mathrm{O}(h^2)$ term after the division by h^2. This proves Eq. (19) and hence (18).

Thanks to (17) we see, that the initialization (8) is just $\mathsf{f}^{(0)}(0,ih)+h\mathsf{f}^{(1)}(0,ih)+h^2\mathsf{f}^{(2)}(0,ih)$. If the population function F_h of the LB algorithm is initialized in such a way, that the initial deviation between the population and the prediction function is of second-order, i.e. $\mathsf{F}_h(0,\cdot,\cdot)-\hat{\mathsf{F}}_h(0,\cdot,\cdot)=\mathrm{O}(h^2)$, then the prediction function $\hat{\mathsf{F}}_h$ is not only *second-order consistent* to the LB equation but to the whole LB algorithm. Observe, that the initialization by (8) is of second-order, if it takes at least the zeroth and first-order term into account.

Now, the LB algorithm is *stable* provided the parameters are reasonably chosen ($0<\omega<2$ and CFL condition, i.e. $1\geqslant |a|/\text{grid speed}=|a|/(h/h^2)=|a|h$). It is well known that consistency and stability imply together convergence. In fact, if we write the LB equation in the form of (18), the stability constant turns out to be *independent* of the grid spacing h. Therefore the order of consistency is equal to the order of the deviation $\mathsf{F}_h(0,\cdot,\cdot)-\hat{\mathsf{F}}_h(0,\cdot,\cdot)$. So we obtain, that the prediction function $\hat{\mathsf{F}}_h$ approximates the population function F_h with second-order accuracy.

$$\mathsf{F}_h(n,i,s)=\hat{\mathsf{F}}_h(n,i,s)+\mathrm{O}(h^2)\equiv\hat{\mathsf{f}}_h(nh^2,ih,s)+\mathrm{O}(h^2). \tag{22}$$

Notice that we could *a posteriori* drop the second and third asymptotic order in the definition of $\hat{\mathsf{f}}_h$; we need them in our argument only for technical reasons to obtain the desired consistency order. Hence $h^2\mathsf{f}^{(2)}+h^3\mathsf{f}^{(3)}$ can now be absorbed into the $\mathrm{O}(h^2)$ term and (22) remains correct if we replace $\hat{\mathsf{F}}_h,\hat{\mathsf{f}}_h$ by $\tilde{\mathsf{F}}_h,\tilde{\mathsf{f}}_h$ with

$$\tilde{\mathsf{F}}_h(n,i,s):=\tilde{\mathsf{f}}_h(nh^2,ih,s):=\mathsf{f}^{(0)}(nh^2,ih,s)+h\mathsf{f}^{(1)}(nh^2,ih,s)\,.$$

Summing (22) over s shows, that the mass-moment of the population function converges quadratically to the solution u of the advection-diffusion equation, i.e.

$$\langle\mathsf{F}_h(n,i),\mathsf{1}\rangle=\sum_{s\in\mathcal{S}}\hat{\mathsf{f}}_h(nh^2,ih,s)+\mathrm{O}(h^2)=u(nh^2,ih,s)+\mathrm{O}(h^2)\,.$$

Using the second equation of (23) (Section 6), we deduce analogously for the first moment and the flux-like quantity f defined in (5)

$$\tfrac{1}{h}\langle\mathsf{F}_h(n,i),\mathsf{s}\rangle=\tfrac{1}{h}\overbrace{\sum_{s\in\mathcal{S}}s\hat{\mathsf{f}}_h(nh^2,ih,s)}^{\langle\hat{\mathsf{f}}_h(nh^2,ih),\mathsf{s}\rangle}+\tfrac{1}{h}\mathrm{O}(h^2)=f(nh^2,ih,s)+\mathrm{O}(h).$$

Actually, this result can be improved, if we construct a prediction function, of at least third-order consistency. Together with the stability, this yields a quadratic convergence of the first moment divided by h, which is in accordance with numerical experiments. If we increase further the consistency order of the prediction function, what requires more regularity, then (11) can be proved in the same manner.

6. APPENDIX B: CONSISTENCY OF THE COUPLING ALGORITHM

Similarly to the previous section we want to construct a prediction function for the LB algorithm on coupled grids. More precisely, we will have separate prediction functions for the population function on each subgrid.

With exception of the four coupling nodes the LB algorithm on the coupled grids is equal to the standard LB algorithm on a uniform grid. Therefore it is natural, if we try the same ansatz as on the uniform grid, setting however $h = r\eta$ on the coarse submesh and $h = \eta$ on the fine submesh.

$$\hat{\mathsf{G}}_\eta(m, j, s) := \hat{\mathsf{f}}_{r\eta}(mr^2\eta^2, jr\eta, s) = \sum_{\alpha=0}^{3} \mathsf{f}^{(\alpha)}(mr^2\eta^2, jr\eta, s)\,(r\eta)^\alpha,$$

$$\hat{\mathsf{K}}_\eta(m, j, s) := \hat{\mathsf{f}}_\eta(m\eta^2, j\eta, s) \qquad = \sum_{\alpha=0}^{3} \mathsf{f}^{(\alpha)}(m\eta^2, j\eta, s)\,\eta^\alpha.$$

The definition of the asymptotic orders $\mathsf{f}^{(\alpha)}$ is the same as in Section 5 (see (16) and (17)). Note, that an iteration on the coarse grid corresponds to a time increment of $r^2\eta^2$, while the time advances on the fine grid only by η^2 after every time step.

We can repeat the computation of the preceeding section to show, that the two prediction functions $\hat{\mathsf{G}}_\eta, \hat{\mathsf{K}}_\eta$ satisfy the LB equation with a residual of order $\mathrm{O}(r^2\eta^2)$, respectively, $\mathrm{O}(\eta^2)$. As r is a fixed quantity independent of η, the residual is actually in both cases of order $\mathrm{O}(\eta^2)$.

Let us now turn to the coupling conditions. Since these are formulated by equalizing certain scaled moments (in our case the zeroth and first one), the specific s-dependence of the asymptotic orders plays a central role. From Eq. (17) we can easily read off

$$\mathsf{f}^{(0)} \propto \mathsf{w}, \quad \mathsf{f}^{(1)} \propto \mathsf{sw}, \quad \mathsf{f}^{(2)} \propto (\mathsf{s}^2 - \tfrac{1}{\theta})\mathsf{w}.$$

It is a crucial fact, that the three vectors $\{\mathsf{w}, \mathsf{sw}, (\mathsf{s}^2 - \frac{1}{\theta})\mathsf{w}\} \subset \mathcal{F}$ occurring in the proportionality relations form together with the set $\{\mathsf{1}, \mathsf{s}, \mathsf{s}^2 - \frac{1}{\theta}\} \subset \mathcal{F}$ a *bi-orthogonal* system with

$$\langle \mathsf{w},\, \mathsf{1}\rangle = 1, \quad \langle \mathsf{sw},\, \mathsf{s}\rangle = \tfrac{1}{\theta}, \quad \left\langle (\mathsf{s}^2 - \tfrac{1}{\theta})\mathsf{w},\, \mathsf{s}^2 - \tfrac{1}{\theta} \right\rangle = \tfrac{1}{\theta} - \tfrac{1}{\theta^2}.$$

In particular this implies:

$$\begin{aligned}
&\langle \mathsf{f}^{(0)},\, \mathsf{1}\rangle = u \qquad \langle \mathsf{f}^{(0)},\, \mathsf{s}\rangle = 0 \qquad \langle \mathsf{f}^{(0)},\, \mathsf{s}^2 - \tfrac{1}{\theta}\rangle = 0,\\
&\langle \mathsf{f}^{(1)},\, \mathsf{1}\rangle = 0 \qquad \langle \mathsf{f}^{(1)},\, \mathsf{s}\rangle = f \qquad \langle \mathsf{f}^{(1)},\, \mathsf{s}^2 - \tfrac{1}{\theta}\rangle = 0,\\
&\langle \mathsf{f}^{(2)},\, \mathsf{1}\rangle = 0 \qquad \langle \mathsf{f}^{(2)},\, \mathsf{s}\rangle = 0 \qquad \langle \mathsf{f}^{(2)},\, \mathsf{s}^2 - \tfrac{1}{\theta}\rangle = -\tfrac{1}{\omega}(1-\theta)g.
\end{aligned}$$

Furthermore we even have $\langle \mathsf{f}^{(3)}, \mathsf{1}\rangle = \langle \mathsf{f}^{(3)}, \mathsf{s}^2 - \frac{1}{\theta}\rangle = 0$, because $\mathsf{f}^{(3)}$ is only composed of terms containing s and $\mathsf{s}^3 = \mathsf{s}$, that are orthogonal to $\mathsf{1},\ \mathsf{s}^2 - \frac{1}{\theta}$. These results can be summarized in the subsequent form, that is exploited further below.

$$\langle \hat{\mathsf{f}}_h, \mathsf{1}\rangle = u, \quad \langle \hat{\mathsf{f}}_h, \mathsf{s}\rangle = hf + \mathrm{O}(h^3), \quad \left\langle \hat{\mathsf{f}}_h, \mathsf{s}^2 - \tfrac{1}{\theta} \right\rangle = -h^2 \tfrac{1}{\omega}(1-\theta)g. \tag{23}$$

After these preparations, we claim, that the first coupling condition is satisfied by the two prediction functions with a residual of fourth-order, whereas the second coupling condition produces a residual of second-order. So the following equations are to be verified (cf. Eq. (13)):

$$\left\langle \tfrac{r^2-\ell}{r^2} \hat{\mathsf{G}}_\eta(n-1, I_\eta^\zeta) + \tfrac{\ell}{r^2} \hat{\mathsf{G}}_\eta(n, I_\eta^\zeta) - \hat{\mathsf{K}}_\eta\big(r^2(n-1)+\ell, J_\eta^\zeta\big),\, \mathsf{1} \right\rangle \stackrel{!}{=} \mathrm{O}(\eta^4), \tag{24}$$

$$\frac{1}{r\eta} \left\langle \tfrac{r^2-\ell}{r^2} \hat{\mathsf{G}}_\eta(n-1, I_\eta^\zeta) + \tfrac{\ell}{r^2} \hat{\mathsf{G}}_\eta(n, I_\eta^\zeta) - r\hat{\mathsf{K}}_\eta\big(r^2(n-1)+\ell, J_\eta^\zeta, \big), \mathsf{s} \right\rangle \stackrel{!}{=} \mathrm{O}(\eta^2). \tag{25}$$

Recall, that we denote by $I_\eta^\zeta, J_\eta^\zeta$ the indices of the two coupling nodes at ζ belonging to the coarse, respectively, fine grid. The time step performed on the coarse grid is indexed by n, while the iterations, which have to be done on the fine grid in between two iterations on the coarse grid to reach the same physical time, are counted by $\ell \in \{1, \ldots, r^2\}$.

Before we substitute in the asserted equations the discrete prediction functions $\hat{\mathsf{G}}_\eta$ and $\hat{\mathsf{K}}_\eta$ by the extended prediction function, let us shortcut $t := (n-1)r^2\eta^2 + \ell\eta^2$. Furthermore remember, that the spatial indices of the coupling nodes have been chosen in such a way that $r\eta I_\eta^\zeta = \eta J_\eta^\zeta = \zeta$. The time interpolation on the coarse grid appearing in both conditions transforms into:

$$\begin{aligned}
&\tfrac{r^2-\ell}{r^2}\,\hat{\mathsf{G}}_\eta(n-1, I_\eta^\zeta) + \tfrac{\ell}{r^2}\,\hat{\mathsf{G}}_\eta(n, I_\eta^\zeta) \\
&\quad = \tfrac{r^2-\ell}{r^2}\,\hat{\mathsf{f}}_{r\eta}(t-\ell\eta^2, \zeta) - \tfrac{\ell}{r^2}\,\hat{\mathsf{f}}_{r\eta}\big(t+(r^2-\ell)\eta^2, \zeta\big) \\
&\quad = \hat{\mathsf{f}}_{r\eta}(t, \zeta) + \mathrm{O}(\eta^4). \qquad (26)
\end{aligned}$$

Let us consider the first coupling condition, Eq. (24), concerning the mass moment. For clarity we drop the arguments (t, ζ). Inserting (26), the left-hand side of (24) becomes:

$$\begin{aligned}
\big\langle \hat{\mathsf{f}}_{r\eta} + \mathrm{O}(\eta^4) - \hat{\mathsf{f}}_\eta,\, \mathsf{1} \big\rangle &= \langle \hat{\mathsf{f}}_{r\eta},\, \mathsf{1}\rangle - \langle \hat{\mathsf{f}}_\eta,\, \mathsf{1}\rangle + \mathrm{O}(\eta^4) \\
&= u - u + \mathrm{O}(\eta^4) = \mathrm{O}(\eta^4).
\end{aligned}$$

In the same way we proceed with the second coupling equation (25) concerning the first moment:

$$\begin{aligned}
\tfrac{1}{r\eta}\big\langle \hat{\mathsf{f}}_{r\eta} + \mathrm{O}(\eta^4) - r\hat{\mathsf{f}}_\eta,\, \mathsf{s} \big\rangle &= \tfrac{1}{r\eta}\big(\langle \hat{\mathsf{f}}_{r\eta},\, \mathsf{s}\rangle - r\langle \hat{\mathsf{f}}_\eta,\, \mathsf{s}\rangle + \mathrm{O}(\eta^4)\big) \\
&= f + \mathrm{O}(r^2\eta^2) - f + \tfrac{1}{r}\mathrm{O}(\eta^2) + \tfrac{1}{r}\mathrm{O}(\eta^3) \\
&= \mathrm{O}(\eta^2).
\end{aligned}$$

So we find (24) and (25) satisfied essentially due to an algebraic property, namely the bi-orthogonality relations between the two $\mathcal{F}$-generating systems. Altogether, the coupling is therefore of second-order.

The consistency check, we have done so far, is the first step towards a convergence proof of the LB algorithm on coupled grids. Starting from the target problem we want to solve, we have constructed prediction functions, that fulfill approximately all equations of the LB algorithm with a residual being at least of order $\mathrm{O}(\eta^2)$. If the algorithm is stable, then the prediction functions approximate moreover the populations on both grids with second-order accuracy, provided that the initial deviation is also of second-order. This would entail immediately the convergence of the algorithm. However, the stability proof is more complicated than in the case of uniform grids and remains an open problem for the general case, even if the examples suggest a good behavior.

Finally, it should be remarked, that the naive approach mentioned in the introduction, where corresponding populations of the coarse and fine grid are simply identified, is only of *first*-order. At the left interface ζ this would mean concretely for instance: $\tilde{\mathsf{G}}_\ominus = \mathsf{K}_\ominus$ and $\mathsf{K}_\oplus = \tilde{\mathsf{G}}_\oplus$. The poor behavior can be understood by means of the prediction functions.

As we assume the asymptotic expansion (22) to be valid *mutatis mutandis* inside the interior of each subdomain, it must also hold by continuity at the interface points:

$$\mathsf{G}_\eta = \mathsf{f}^{(0)} + r\eta\mathsf{f}^{(1)} + \mathrm{O}(\eta^2),$$
$$\mathsf{K}_\eta = \mathsf{f}^{(0)} + \eta\mathsf{f}^{(1)} + \mathrm{O}(\eta^2).$$

For ease of notation, we have omitted the arguments. Obviously, the populations on the coarse and fine grid differ in the first-order by the factor r. Hence we commit an error of order $\mathrm{O}(\eta)$, if we "copy" the values of corresponding populations from the coarse to the fine grid and vice versa for $r \neq 1$.

ACKNOWLEDGMENTS

I thank Prof. M. Junk from the Universität Konstanz for valuable and stimulating discussions.

REFERENCES

1. G. McNamara and G. Zanetti, Use of the Boltzmann equation to simulate lattice-gas automata, *Phys. Rev. Lett.* **61**:2332 (1988).
2. D. A. Wolf-Gladrow, Lattice-Gas Cellular Automata and Lattice-Boltzmann Models. Springer, Lecture Notes in Mathematics 1725, Heidelberg 2000.
3. O. Filippova and D. Hänel, Boundary-fitting and local grid refinement for Lattice-BGK models, *Int. Jo. Mod. Phys. C*, **9**(8):1271–1279 (1998).
4. O. Filippova and D. Hänel, Grid refinement for Lattice-BGK models, *J. Comput. Phys.* **147**:219–228 (1998).
5. O. Filippova and D. Hänel, Acceleration of Lattice-BGK schemes with grid refinement, *J. Comput. Phys.* **165**:407–427 (2000).
6. B. Crouse, E. Rank, M. Krafczyk, and J. Tölke, A LB-based approach for adaptive flow simulations, *Int. J. Modern Phys. B*, **17**(1–2):109–112 (2003).
7. M. Krafczyk, Gitter-Boltzmann-Methoden: Von der Theorie zur Anwendung. Habilitationsschrift, TU München 2001, www.cab.bau.tu-bs.de/forschung/veroeffentlichungen/habilitationen.htm.
8. A. Dupuis and B. Chopard, Theory and applications of an alternative Lattice-Boltzmann grid refinement algorithm, *Phys. Rev. E* **67**:066707 (2003).
9. M. Junk, A. Klar and L.-S. Luo, Asymptotic Analysis of the Lattice-Boltzmann equation, preprint to appear.
10. M. Junk and Z. Yang, Asymptotic Analysis of Lattice-Boltzmann Boundary Conditions, preprint to appear.
11. M. Junk and W. Yong, Rigorous Navier-Stokes limit of the lattice Boltzmann equation, *Asymptotic Anal.* **35**:165–185 (2003).
12. M. Rheinländer, PhD thesis to appear.